ACS OMEGA

http://pubs.acs.org/journal/acsodf

Article

Functionalized MOF-Derived Nanoporous Carbon as Compatible Nanofiller to Fabricate Defect-Free PDMS-Based Mixed Matrix Pervaporation Membranes

Xu Zhang,[§] Zhaowei Tong,[§] Chao Liu, Lei Ye, Yuwei Zhou, Qin Meng,* Guoliang Zhang,* and Congjie Gao

Cite This: *ACS Omega* 2022, 7, 15786−15794

Read Online

ACCESS | Metrics & More | Article Recommendations | Supporting Information

ABSTRACT: Metal−organic framework (MOF)-based polydimethylsiloxane mixed matrix membranes applied for alcohol recovery with high permeability and selectivity are drawing more and more attention. However, the design and fabrication of high-quality and stable MOF-based mixed matrix membrane for pervaporation are still a big challenge. Herein, PDMS functionalized MOF-derived nanoporous carbon (P-ZNC) was first explored as compatible nanofiller to mutually blend with polydimethylsiloxane on PVDF substrate to fabricate defect-free mixed matrix membranes via dip-coating and thermal cross-linkng. Induced by UV illumination, hydrophobic modification of MOF-derived nanoporous carbon was successfully realized under mild conditions within one step, simplifying the operation step. By using this facile strategy, we can not only solve the existing problem of agglomeration, but also covalently cross-link MOF derivative with polymeric matrix and effectively eliminate the interface defect between polymer and nanoparticles without any extra steps. The method also gives a good level of generality for the synthesis of versatile stable nanoporous MOF-derived carbon-based mixed matrix membranes on various supports. The prepared PDMS/P-ZNC with commendable structures possessed excellent separation performance in low concentration *n*-butanol recovery and had a good balance between permeance, selectivity, and stability.

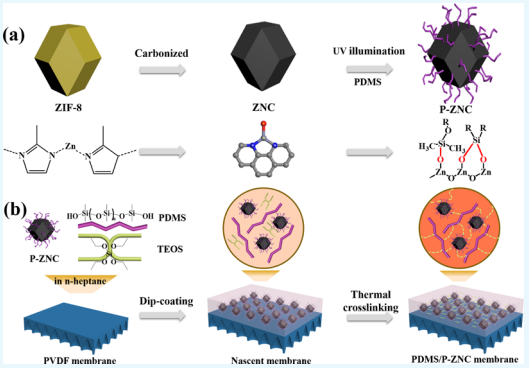

1. INTRODUCTION

Pervaporation (PV), as a promising membrane separation technology, has been successfully applied in recovering dilute biobutanol from fermentation broth due to the unique advantages of simple process, low energy consumption without secondary pollution, and restriction of vapor−liquid equilibrium.[1,2] To obtain an organophilic PV membrane for recovering butanol with a low concentration, polydimethylsiloxane (PDMS) is the currently used material because of its high hydrophobicity, excellent chemical stability, and good thermal properties.[3−7] However, the separation performance of the PDMS membrane is limited by the mutual restriction between permeability and selectivity,[8−10] restricting the further application of the PDMS membrane. Recently, doping hydrophobic nanoparticles such as metal organic frameworks (MOFs) into the PDMS matrix to prepare mixed matrix membranes (MMMs) turns out to be an effective way to break through the bottleneck.[11−15] MOFs, as a new type of crystalline material, are excellent fillers with high specific surface area and designable structure and pore size for preparing MMMs.[16−19] Although these membranes combine the advantages of PDMS and MOFs and improve the pervaporation performance to some extent, the acid by-products in practical fermentation broth may destroy the structure of MOFs,[20,21] affecting the long-term stability and limiting the application of MOF-based MMMs in recovering butanol. Search for new and stable nanofillers is important to fabricate high-performance PV membranes.

Carbon materials have better thermal and chemical stability and are widely used in various areas including catalysis, energy storage, and adsorption.[22,23] Compared to other templates, MOFs are considered as promising templates to synthesize nanoporous carbon materials for their structural features. By taking advantage of MOFs, MOF-derived nanoporous carbons not only directly inherit the hierarchical pore structure and flexible framework of MOFs but also possess the unique stability of carbon materials,[24−31] which will be important candidates to fabricate stable MMMs with good separation performance. However, the intrinsic inorganic property of carbon materials may lead to poor compatibility with PDMS

Received: February 13, 2022
Accepted: April 4, 2022
Published: April 26, 2022

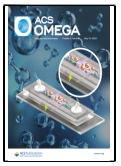

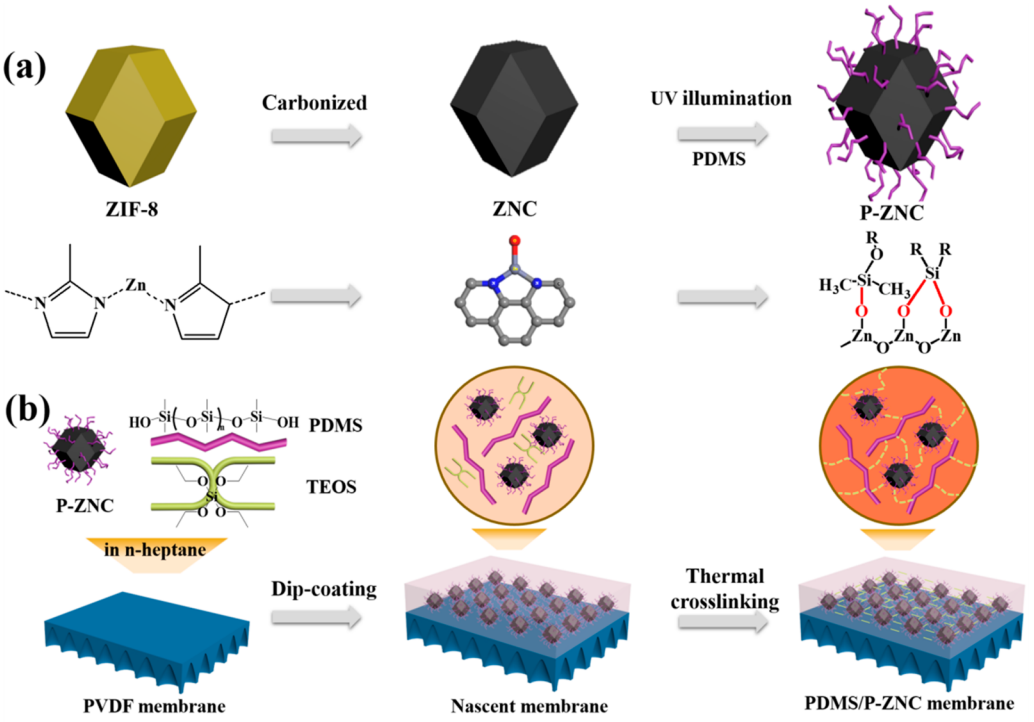

Figure 1. Schematic illustration. (a) Synthesis of MOF-derived nanoporous carbon P-ZNC nanoparticles. (b) Preparation of PDMS/P-ZNC mixed matrix pervaporation membrane.

matrix, forming interfacial defects and failing to achieve high-quality MMMs.[12,32] Therefore, the combination of MOF-derived nanoporous carbons and hydrophobic modification should be very critical to obtain sufficient compatibility with PDMS for fabricating high-quality mixed matrix pervaporation membranes.

Based on the above analyses, herein, we have designed PDMS functionalized MOF-derived nanoporous carbon (P-ZNC) as compatible nanofiller and mutually blended with PDMS through covalent cross-linking by using a new and facile synthetic method. The high-quality PDMS/P-ZNC mixed matrix pervaporation membranes can be synthesized easily on the polymer substrate (Figure 1). For carbon materials, they usually need to oxidize the carbon materials to construct a carboxyl group as reactive site under harsh condition, and then carry out grafting hydrophobic molecules.[33,34] The related functionalization process usually consists of very complicated multistep reactions and increases environmental burdens. Unconventionally, hydrophobic modification of ZNC in this work was carried out under relatively mild UV-induced condition within one step, simplifying the operation steps (Figure S1). According to the solubility parameter close principle, the ZNC modified with PDMS has good compatibility with the PDMS matrix, greatly eliminating the agglomeration of nanoparticles. Moreover, different from the conventional simple blending method without forming a chemical bond between the polymer and nanoparticles, the PDMS part of P-ZNC nanoparticles reacts with the tetraethyl orthosilicate (TEOS) to covalently cross-link the polymeric matrix, effectively eliminating the interface defect between polymer and nanoparticles (Figure S2). Further, the introduction of hydrophobic P-ZNC not only increases hydrophobicity of the PDMS based membrane but also provides additional transport channel, enhancing the pervaporation performance.

2. EXPERIMENTAL SETUP

2.1. Materials. *n*-Butanol, methanol, *n*-heptane, tetraethyl orthosilicate (TEOS), dibutyltin dilaurate (DBTDL), and zinc nitrate hexahydrate ($(Zn(NO_3)_2{\cdot}6H_2O)$) were supplied by Sinopharm Chemical Co. Ltd., China. 2-Methylimidazole (Hmim) was purchased from Aladdin Co., Ltd., China. The deionized water (ion contents $\sigma \leq 0.5\ \mu S\ cm^{-1}$) is purified by RO/EDI equipment. The poly(vinylidene fluoride) (PVDF) ultrafiltration membrane (molecular weight cutoff of 50 000 Da) was obtained from Rising Sun Membrane Technology (Beijing) Co. Ltd., China. Polydimethylsiloxane (PDMS, viscosity of 10 000 mPa·s) was purchased from Xingfeilong Chemical Co. Ltd., China.

2.2. Preparation of ZIF-8 Nanoparticles. Zn^{2+} solution was prepared by dissolving $Zn(NO_3)_2{\cdot}6H_2O$ (0.7348 g) in 50 mL methanol, and Hmim solution was prepared by dissolving 2-methylimidazole (0.8112 g) in methanol (50 mL). Zn^{2+} solution was thoroughly mixed with Hmim solution under stirring and then continued to stir for 10 min and left to stand for 24 h. Then, the resulting ZIF-8 nanoparticles were collected from the mixed solution and washed with methanol three times. The nanoparticles were vacuum-dried at 80 °C overnight.

2.3. Preparation of ZNC Nanoparticles. ZNC nanoparticles were prepared by carbonizing ZIF-8 under high temperature. In detail, ZIF-8 was carbonized at 800 °C under the condition of nitrogen flow for 8 h. The resulting black powder was ZNC nanoparticles.

2.4. Preparation of P-ZNC Nanoparticles. As in typical priming, PDMS and ZNC nanoparticles were dispersed into *n*-heptane via stirring. The concentration of PDMS in *n*-heptane

https://doi.org/10.1021/acsomega.2c00881
ACS Omega 2022, 7, 15786−15794

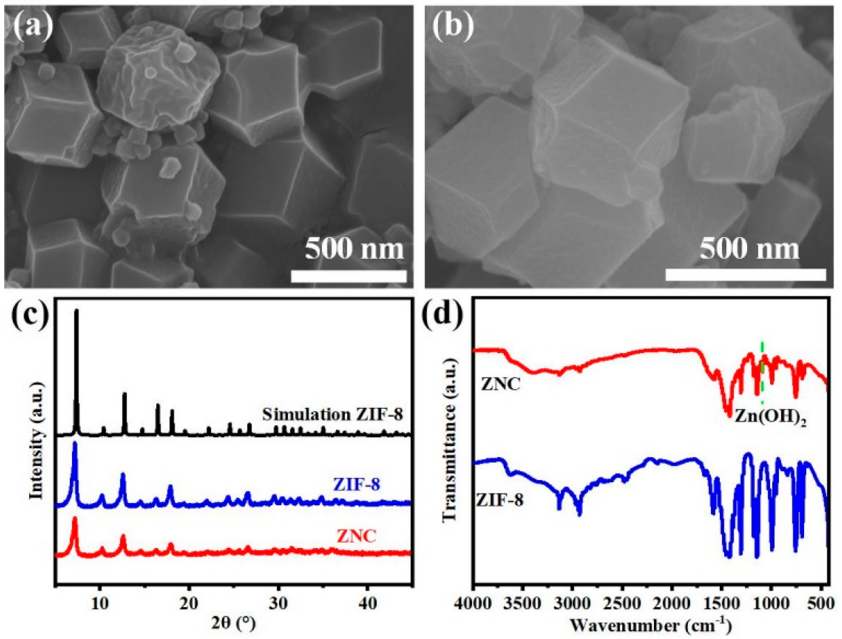

Figure 2. SEM images of ZIF-8 (a) and ZNC (b), XRD patterns (c), and FTIR spectra (d) of ZIF-8 and ZNC nanoparticles.

solution was 1 wt %. The loading capacity of ZNC in the ZNC/PDMS mixture ranged from 1 to 10 wt % (ZNC/PDMS, w/w). After dispersing ZNC in PDMS solution, the solution was irradiated with ultraviolet (UV) light to induce PDMS grafting on ZNC. Then, the P-ZNC nanoparticles were obtained and uniformly dispersed in PDMS solution.

2.5. PDMS/P-ZNC Membrane Preparation. Catalyst (DBTDL, 2 wt %) and cross-linking agent (TEOS, 0.1 wt %) were directly added into the PDMS solution containing P-ZNC under stirring to get a coating solution. Then, the poly(vinylidene fluoride) (PVDF) substrate was horizontally immersed into the coating solution to form a nascent membrane. The PDMS/P-ZNC membrane was synthesized for thermal cross-linking at 80 °C overnight.

2.6. PDMS/ZNC Membrane Preparation. The fabrication of the PDMS/ZNC membrane was similar to that of the PDMS/P-ZNC membrane. The only difference was that the PDMS solution containing ZNC nanoparticles without UV irradiation directly added catalyst and cross-linking agent to get a coating solution.

2.7. Membrane Characterization. In order to observe the morphology of ZIF-8 particles and ZNC particles as well as the morphology including the surface and section of membranes, field emission scanning electron microscopy (SEM, Hitachi S-4700) was used. The energy-dispersive X-ray (EDX) detector loaded by SEM carried out the elemental analysis of the membrane surface. The membrane sample is fractured in liquid nitrogen to obtain the sample cross section. All the samples were sprayed with gold in vacuum to improve their electrical conductivity. The particle sizes of ZIF-8 and ZNC were measured by particle size separation instrument (NanoBrook Omni), and the particle size changes before and after carbonization were analyzed. The powder was analyzed by XRD using X'Pert PRO diffractometer (Panaco, Netherlands). X-ray photoelectron spectroscopy (XPS, Kratos Axis Ultra) was used to characterize the chemical elemental composition. The scanning range was 5−50, and the step length was 0.02 min. Fourier transform infrared spectroscopy (FTIR, Nicolet-6700, Thermo Scientific, USA) was used to study the chemical structure characteristics of the membrane and nanoparticles. The water contact angles of PDMS/P-ZNC MMMs and original PDMS films were measured by contact angle analyzer (Oceana15EC, Data Physics) to characterize their hydrophobicity. The images were taken after 3 μL of water was held on the membrane surface for 10 s. Each membrane was measured in four different positions to ensure accuracy.

2.8. PV Experiments. PV testing of the PDMS membrane and PDMS/P-ZNC membrane was carried out by a self-made plate and a frame pervaporation device. A peristaltic pump was used to keep the feed flow at 240 mL min^{-1}, and a magnetic stirring constant temperature water bath was used to adjust the feed temperature. The vacuum pump worked continuously to ensure that the permeation side steam was removed, and a vacuum gauge was used to monitor the negative pressure. The steam on the permeation side was trapped in the cold trap (liquid nitrogen cooling). The PV properties of MMMs were tested at different temperatures (40−80 °C) and the same temperature (60 °C) with different feed liquid concentration. After the experimental equipment was operated for 1 h and reached the stable state, sampling was started. A small amount of acetone was added to the sample to ensure that the components were well mixed and then the sample was quantified by a gas chromatograph (GC 1102).

The permeability of the pervaporation membrane can be characterized by the total flux (J), and the selectivity can be described by the separation factor (α), which can be calculated as follows: The permeability and selectivity of pervaporation membranes can be characterized by the two factors of pervaporation flux and separation factor. The total flux (J) and separation factor (α) of the membrane are calculated as follows:

$$J = \frac{m}{A \times t} \quad (1)$$

https://doi.org/10.1021/acsomega.2c00881
ACS Omega 2022, 7, 15786−15794

$$\alpha = \frac{Y/(1-Y)}{X/(1-X)} \quad (2)$$

where m (g) is the total mass of the collected permeate in the cold trap, t (h) is the collection time, A (m^2) represents the effective membrane area (7 cm^2), and X and Y represent the n-butanol concentration in feed and permeation solution, respectively.

2.9. Solvent Uptake Test. The interaction between the permeable component and the pervaporized membrane can be understood by the solvent uptake test. Before the test, the samples were dried at 80 °C for 24 h. After drying, the mass of each membrane was accurately weighed, and then the membrane samples were placed in pure water and 5 wt % n-butanol aqueous solution, respectively. After soaking for 48 h, the sample membrane was removed, the residual water or solution on the surface of the film was quickly cleaned off, and the sample was quickly weighed. The calculation formula of the solvent uptake of the membrane is as follows:

$$\text{solvent uptake}(\%) = \frac{m_s - m_d}{m_d} \times \text{oven} \quad (3)$$

where m_d and m_s, respectively, represent the weight of membrane samples before and after immersion.

3. RESULTS AND DISCUSSION

The preparation process of MOF-derived nanoporous carbon P-ZNC nanoparticles is illustrated in Figure 1a. After carbonization of ZIF-8 particles, the morphology of the ZNC nanoparticles was a rhomboid dodecahedron structure, which was relatively complete and inherited the crystal structure of ZIF-8 (Figure 2a and b). The average particle size of ZNC nanoparticles was 413.9 nm and was smaller than that of ZIF-8 (465.7 nm) (Figure S3). The reason for the size reduction of ZNC nanoparticles was that the structure of the porous carbon nanoparticles shrunk slightly during the process of high-temperature calcination. ZIF-8 and ZNC nanoparticles were characterized by XRD to understand the changes of ZIF-8 nanoparticles before and after calcination, and the results are shown in Figure 2c. The diffraction peak of obtained ZNC was consistent with peaks of ZIF-8, which showed that ZNC retained the original crystal structure of ZIF-8.[35] FTIR was used to analyze the chemical construction of ZIF-8 and ZNC (Figure 2d). For ZIF-8 nanoparticles, the spectral band in the range of 1550−600 cm^{-1} is the stretching vibration and bending vibration absorption peaks of the imidazole ring, and the spectral band at 422 cm^{-1} is the stretching vibration of the Zn−N ring.[36] For ZNC, a new peak appeared at 1135 cm^{-1}, corresponding to the vibration absorption peak of the amphoteric zinc hydroxide hydroxyl group.[37] It can be inferred that ZnO was generated after the calcination of ZIF-8, and the water from the atmospheric environment adsorbed on the surface of ZnO to form $Zn(OH)_2$ which provided active sites for further functionalization. The ZNC were dispersed in PDMS solution and irradiated with ultraviolet (UV) light to obtain P-ZNC which grafted PDMS. From S4, the Si−O−Zn bond (531.3 eV), resulting from the grafting of PDMS on the ZNC surface, was revealed.[38] A sedimentation test of ZNC and P-ZNC in PDMS solution was run (Figure S5). The result showed that ZNC settled rapidly within 20 min, while modified P-ZNC remained suspended, indicating that the surface grafting rather than physical deposition of PDMS effectively improved the dispersibility of ZNC.

The PDMS/P-ZNC membrane was prepared on the PVDF substrate by the dip-coating method (Figure 1b). The morphologies of PDMS/P-ZNC and PDMS membranes were characterized by SEM (Figure 3). After introducing P-ZNC nanoparticles, there was no visible agglomeration of the PDMS/P-ZNC membrane after incorporating P-ZNC nanoparticles. From Figure 3c and d, it can be found that the thickness of the selective layer of PDMS/P-ZNC membrane is 16.0 μm, which is lower than that of PDMS membrane (22.6 μm). This may be because the molecular chain of PDMS became shorter, and the viscosity of P-ZNC dispersions decreased during the UV grafting reaction. In addition, the Zn element was well distributed (Figure 4), indicating that P-ZNC was uniformly distributed in the PDMS matrix. The excellent compatibility of the PDMS/P-ZNC membrane may be a resulted of the covalent link between the PDMS matrix and P-ZNC eliminating the interfacial defects between P-ZNC and the PDMS matrix.

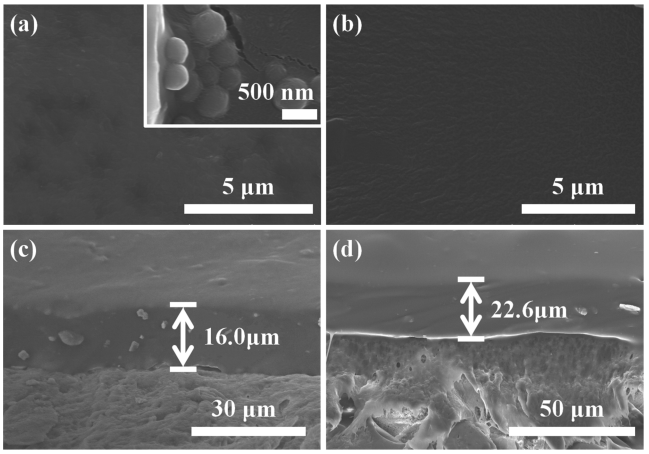

Figure 3. Surface and cross-section SEM images of PDMS/P-ZNC (a, c) and PDMS (b, d) membranes.

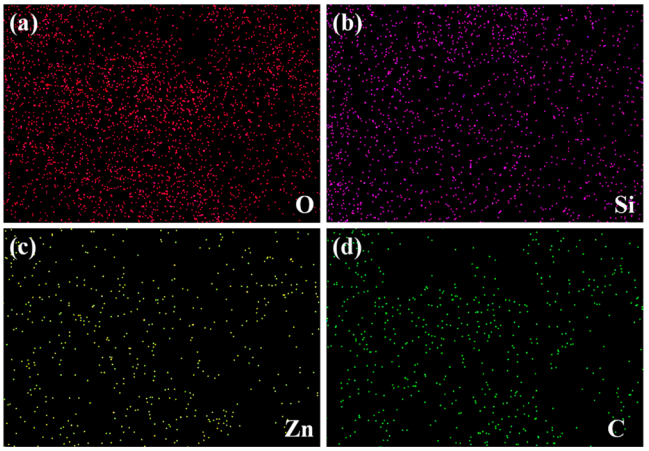

Figure 4. EDXS mapping of PDMS/P-ZNC membrane: (a) O, (b) Si, (c) Zn, and (d) C.

To confirm the successful grafting of PDMS, FTIR was used to analyze the chemical structure of PDMS and PDMS/P-ZNC membranes (Figure 5). For pristine PDMS membrane, the characteristic peak at 1257 cm^{-1} corresponds to the symmetric bending vibration of $-CH_3$ in Si-CH_3, the

https://doi.org/10.1021/acsomega.2c00881
ACS Omega 2022, 7, 15786−15794

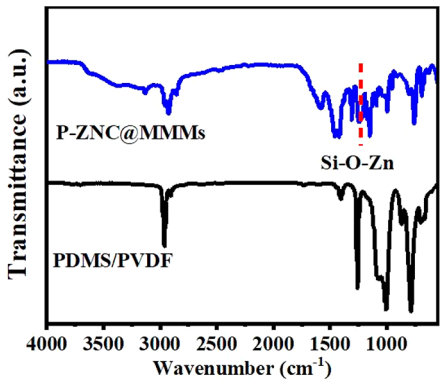

Figure 5. FTIR spectra of PDMS and PDMS/P-ZNC membranes.

characteristic peak at 1007 cm^{-1} corresponds to the stretching vibration of Si−O−Si, and the characteristic peak at 786 cm^{-1} corresponds to the stretching vibration of $-CH_3$ in Si-CH_3. Compared with the PDMS membrane, the peak area of the PDMS/P-ZNC membrane at 909 cm^{-1} significantly increased, corresponding to the Si−O−Zn stretching vibration, proving that chemical cross-linking between PDMS and ZNC nanoparticles occurred.[39] In addition, after immersing the PDMS/ZIF-8 and PDMS/P-ZNC membranes into 4 g/L acetic acid for 12 h, it was found that the PDMS/ZIF-8 membrane formed a pinhole, but the PDMS/P-ZNC membrane still retained its integrity and had no defects (Figure 6), showing that the PDMS/P-ZNC membrane had better acid-stability.

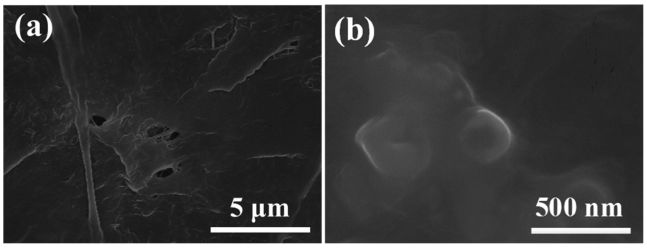

Figure 6. SEM images of PDMS/ZIF-8 (a) and PDMS/P-ZNC (b) membranes after immersing into 4 g/L acetic acid for 12 h.

The influence of P-ZNC on the hydrophobicity of PDMS membranes was investigated. From Figure 7, it is obvious that the P-ZNC had a positive effect on the hydrophobicity of PDMS/P-ZNC membrane and generally increased with the

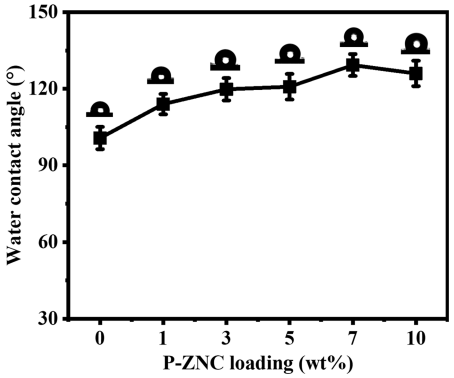

Figure 7. Static water contact angle of PDMS/P-ZNC membranes with different loading.

increase of P-ZNC loading. When the P-ZNC loading amount of PDMS/P-ZNC membrane was 7 wt %, the water contact angle reached the maximum of 129.3 ± 3.2°, which was much higher than that of the original PDMS membrane (100.7 ± 3.3°). However, when the doping amount further reached 10 wt %, the water contact angle of PDMS/P-ZNC membrane decreased to 126.0 ± 4.0°, maybe resulting from the inevitable accumulation of P-ZNC nanoparticles leading to the extensive change of surface property. The swelling experiments of membranes in pure water and 5 wt % *n*-butanol aqueous solution were tested (Figure 8). The swelling degree of the

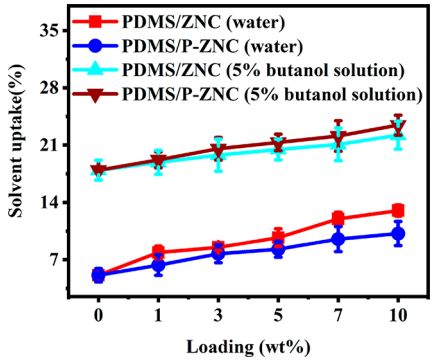

Figure 8. Solvent uptake of pure PDMS membrane and PDMS/P-ZNC membrane in water and 5.0 wt % butanol solution.

membrane in *n*-butanol solution was greater than that in water solution, because the hydrophobic PDMS selective layer had better affinity toward butanol. Compared with the original PDMS membrane, introduction of both ZNC and P-ZNC nanoparticles into the PDMS matrix increased the hydrophobicity of the resulting membranes. The swelling degree of PDMS-based membranes were in the sequence of PDMS/P-ZNC > PDMS/ZNC > PDMS membrane. ZNC modified by PDMS has enhanced hydrophobicity of PDMS-based membranes, further increasing the affinity toward butanol and improving the swelling degree of membranes.

The effect of MOF-derived nanoporous carbon on the pervaporation performance of PDMS-based membranes was tested for separating a 1 wt % butanol solution at 60 °C. For the pristine PDMS membrane, the total flux was 675.2 g m^{-2} h^{-1} and the separation factor was 33.7. After incorporating ZNC nanoparticles, although the total flux of PDMS/ZNC membranes increased up to 837.8 g m^{-2} h^{-1}, the selectivity slightly decreased by 8.7% to 30.8 (Figure 9). Because the permeable components entered into the membrane and preferentially passed through the pores of ZNC quickly,

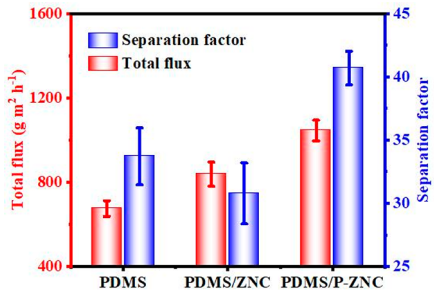

Figure 9. PV performance of pure PDMS, PDMS/ZNC, and PDMS/P-ZNC membranes.

https://doi.org/10.1021/acsomega.2c00881
ACS Omega 2022, 7, 15786−15794

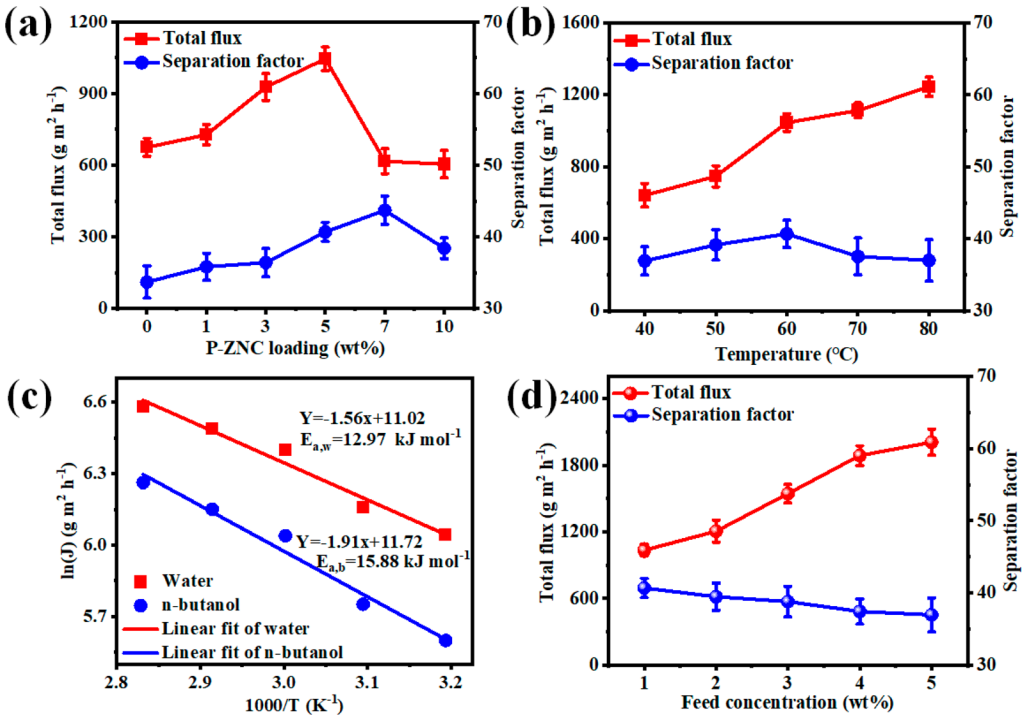

Figure 10. (a) PV performance of PDMS/P-ZNC membranes with different loading. (b) Effect of feed temperature on PV performance of PDMS/P-ZNC membrane. (c) Arrhenius curve of flux for *n*-butanol and water. (d) Effect of feed temperature on pervaporation performance of PDMS/P-ZNC membrane.

membrane flux improved. The decrease of separation factor may be due to the poor compatibility between ZNC and the PDMS matrix, leading to an increase in the nonselective defects, thus reducing the selectivity of the PDMS/ZNC membrane. Compared with the PDMS/ZNC membrane, the flux and separation factor of the PDMS/P-ZNC membrane were further improved to 1035.4 g m^{-2} h^{-1} and 40.7, respectively. Compared with ZNC, the PDMS-modified ZNC (P-ZNC) exhibited a lower BET surface area, total pore volume, and micropore volume, owing to the pores being partially occupied by PDMS. Thus, compared with the pure membrane, the total flux of PDMS/ZNC slightly increased. For the PDMS/P-ZNC membrane, even though the BET surface area, total pore volume, and micropore volume of P-ZNC further decreased, the ZNC nanoparticles modified by PDMS had better affinity with PDMS and dispersed more uniformly in the PDMS matrix, avoiding the agglomeration of nanoparticles and improving the separation performance of the PDMS/P-ZNC membrane. Moreover, compared with the PDMS membrane, the PDMS/P-ZNC membrane presented better separation performance with the separation factor and flux increased by 20.7% and 53.3%, respectively. The separation performance of PDMS/P-ZNC membranes with different loading was further demonstrated (Figure 10a). With increasing loading of P-ZNC, the flux and separation factor of PDMS/P-ZNC membranes increased first and then decreased. The strong hydrophobicity of P-ZNC made butanol preferentially diffused into the inner selective layer, thus increasing the selectivity of the membrane. When P-ZNC loading was 7 wt %, the separation factor of the PDMS/P-ZNC membrane reached the maximum of 43.5. However, when the loading was too large, P-ZNC agglomeration would inevitably occur in the membrane, resulting in the increase of nonselective defects in the membrane and thus reducing the selectivity of the membrane. Meanwhile, the flux of PDMS/P-ZNC membranes had the similar phenomena of the separation factor.

As illustrated in Figure 10b and Figure S6, with the increase of the feed liquid temperature, the total flux showed an increasing trend from 641.7 to 1245.6 g m^{-2} h^{-1}, and the separation factor increased from 36.9 to 40.7. To investigate the effect of feed temperature on the total flux, the Arrhenius equation was applied (Figure 10c).[39] It can be concluded that the increase of temperature contributed to the increase of flux and the increase of the transmembrane vapor pressure difference of each component at a higher temperature, which improved the transport driving force. According to the formula, the apparent activation energy of *n*-butanol and water was 15.9 and 13.0 kJ mol^{-1}, respectively.[40] The higher apparent activation energy indicated that water membrane permeability was more sensitive to temperature. Therefore, the butanol flux of membrane increased faster than water flux with the increase of temperature. Evaporation enthalpy was also extracted from the apparent activation energy to calculate the osmotic activation energy. Evaporation enthalpy is extracted from the apparent activation energy to calculate the osmotic activation energy $E_{p,i}$ of component i:[41]

$$E_{p,i} = E_{a,i} - \Delta H_{exp,i} \quad (4)$$

where $\Delta H_{evp,i}$ is the enthalpy of evaporation of the component i, $\Delta H_{evp,i}$ of the water and *n*-butanol are $\Delta H_{evp,w}$ = −42.8 kJ mol^{-1} and $\Delta H_{evp,w}$ = 43.7 kJ mol^{-1}. $E_{p,i}$ can also be expressed by the following formula:

$$E_{p,i} = \Delta H_{s,i} + E_{D,i} \quad (5)$$

where $\Delta H_{s,i}$ represents the i enthalpy of dissolution, $E_{D,i}$ is the diffusion activation energy of component i. The osmotic activation energies of the effluent and *n*-butanol were

https://doi.org/10.1021/acsomega.2c00881
ACS Omega 2022, 7, 15786−15794

calculated as −30.3 and −29.8 kJ mol^{-1}, respectively. Since the pervaporation process of a two-component system such as water and butanol is an exothermic process, we can conclude that the dissolution process is the rate-controlling step of pervaporation. Thus, when the feed temperature increased, butanol which was more sensitive to temperature than water dissolved preferentially, leading to improvement in the separation factor. At temperatures above 60 °C, butanol flux increased more slowerly than water flux, showing that water diffusion played a dominant role and thus resulted in the separation factor decrease. The influence of feed concentration was also studied. As feed *n*-butanol concentration increased, the total flux of PDMS/P-ZNC membrane increased linearly from 1035.4 to 2007.1 g m^{-2} h^{-1}, but the separation factor decreased gradually from 40.7 to 36.9 (Figure 10d). This is due to the synergistic effect of the driving force and membrane expansion.[42,43] At the same time, the free volume and the elasticity of the polymer chain increased, enhancing the ability of water to penetrate the membrane, so the total flux continued to increase. Compared with other carbon-based MMMs, PDMS/P-ZNC MMMs possessed both competitive flux and separation factor (Table S2) and had good long-term stability (Figure 11). Moreover, according to the mechanism of our strategy, defect-free PDMS-based MMMs incorporating other UV-induced modified MOFs such as ZIF-67 derived porous carbon can also be prepared (Figure S7).

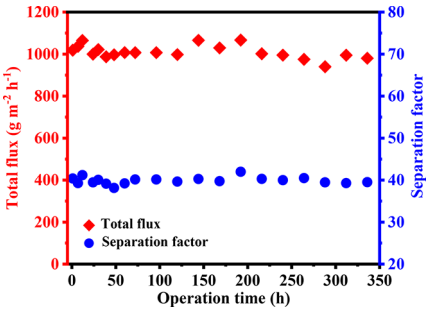

Figure 11. Long-term PV performance of PDMS/P-ZNC membrane for separating 1.0 wt % butanol solution at 60 °C.

4. CONCLUSIONS

In summary, we report a new dip-coating and thermal cross-linkng method to fabricate defect-free PDMS-based MMMs by using functionalized MOF-derived nanoporous carbon as a compatible nanofiller. Unlike previous reports, hydrophobic modification of ZNC under mild UV-induced conditions avoided complicated multistep reactions and related environmental burdens. Since functionalized ZNC had good compatibility with the PDMS matrix, the agglomeration problem can be solved. Moreover, different from the simple blending method, P-ZNC covalently the cross-linked polymeric matrix and effectively eliminated the interface defect between polymer and nanoparticles. The prepared PDMS/P-ZNC membranes with enhanced hydrophobicity had commendable structures and acid stability and exhibited excellent permeation flux and separation factor toward dilute *n*-butanol solution. When the loading amount was 7 wt %, the total flux of the resulted PDMS/P-ZNC membrane reached 1035.4 g m^{-2} h^{-1}, the separation factor was 40.7, which was 20.7% and 53.3% higher than that of the pure PDMS membrane, respectively; and as the feed *n*-butanol temperature increased, the total flux of the PDMS/P-ZNC membrane further increased to 1245.6 g m^{-2} h^{-1}. In addition, our strategy displays a great applicability and can be engaged in synthesizing versatile MOF-based mixed matrix membranes on different substrates, which offers good opportunities for facile construction of stable and uniform MOF-derived composite membranes.

■ ASSOCIATED CONTENT

Supporting Information

The Supporting Information is available free of charge at https://pubs.acs.org/doi/10.1021/acsomega.2c00881.

Additional synthesis route, size distribution of ZIF-8 and ZNC, and the performance comparison of as-fabricated PDMS/P-ZNC membrane with other carbon-based PV MMMs (PDF)

■ AUTHOR INFORMATION

Corresponding Authors

Guoliang Zhang − *Center for Membrane and Water Science & Technology, Institute of Oceanic and Environmental Chemical Engineering, State Key Lab Breeding Base of Green Chemical Synthesis Technology, Zhejiang University of Technology, 310014 Hangzhou, China;* orcid.org/0000-0002-7371-3349; Phone: +86-571-88320863; Email: guoliangz@zjut.edu.cn

Qin Meng − *College of Chemical and Biological Engineering, and State Key Laboratory of Chemical Engineering, Zhejiang University, 310027 Hangzhou, China;* orcid.org/0000-0002-8017-6852; Phone: 86-571-87953193; Email: mengq@zju.edu.cn; Fax: 86-571-87951227

Authors

Xu Zhang − *Center for Membrane and Water Science & Technology, Institute of Oceanic and Environmental Chemical Engineering, State Key Lab Breeding Base of Green Chemical Synthesis Technology, Zhejiang University of Technology, 310014 Hangzhou, China*

Zhaowei Tong − *Center for Membrane and Water Science & Technology, Institute of Oceanic and Environmental Chemical Engineering, State Key Lab Breeding Base of Green Chemical Synthesis Technology, Zhejiang University of Technology, 310014 Hangzhou, China*

Chao Liu − *Center for Membrane and Water Science & Technology, Institute of Oceanic and Environmental Chemical Engineering, State Key Lab Breeding Base of Green Chemical Synthesis Technology, Zhejiang University of Technology, 310014 Hangzhou, China*

Lei Ye − *Center for Membrane and Water Science & Technology, Institute of Oceanic and Environmental Chemical Engineering, State Key Lab Breeding Base of Green Chemical Synthesis Technology, Zhejiang University of Technology, 310014 Hangzhou, China*

Yuwei Zhou − *Center for Membrane and Water Science & Technology, Institute of Oceanic and Environmental Chemical Engineering, State Key Lab Breeding Base of Green Chemical Synthesis Technology, Zhejiang University of Technology, 310014 Hangzhou, China*

Congjie Gao − *Center for Membrane and Water Science & Technology, Institute of Oceanic and Environmental Chemical Engineering, State Key Lab Breeding Base of Green*

https://doi.org/10.1021/acsomega.2c00881
ACS Omega 2022, 7, 15786−15794

Chemical Synthesis Technology, Zhejiang University of Technology, 310014 Hangzhou, China

Complete contact information is available at: https://pubs.acs.org/10.1021/acsomega.2c00881

Author Contributions

[§]X.Z. and Z.T. contributed equally.

Notes

The authors declare no competing financial interest.

■ ACKNOWLEDGMENTS

We are thankful for financial support from the National Natural Science Foundation of China (21736009 and 21808202), the Zhejiang Provincial Bureau of Science and Technology, China (Grants No. 2021C03169), SINOPEC Science and Technology Development Project from China Petrochemical Corporation (No. 33750000-20-ZC0607-0012 and 33750000-21-ZC0607-0005), and Tongjiang Scholarship from Fujian Quanzhou Government.

■ REFERENCES

(1) Kujawska, A.; Kujawski, J.; Bryjak, M.; Kujawski, W. Renew. ABE Fermentation Products Recovery Methods-A Review. *Renew. Sust. Energy Rev.* **2015**, *48*, 648−661.

(2) Ong, Y. K.; Shi, G. M.; Le, N. L.; Tang, Y. P.; Zuo, J.; Nunes, S. P.; Chung, T.-S. Recent Membrane Development for Pervaporation Processes. *Prog. Polym. Sci.* **2016**, *57*, 1−31.

(3) Fan, H.; Wang, N.; Ji, S.; Yan, H.; Zhang, G. Nanodisperse ZIF-8/PDMS Hybrid Membranes for Biobutanol Permselective Pervaporation. *J. Mater. Chem. A* **2014**, *2*, 20947−20957.

(4) Sun, L.; Baker, G. L.; Bruening, M. L. Polymer Brush Membranes for Pervaporation of Organic Solvents from Water. *Macromolecules* **2005**, *38*, 2307−2314.

(5) Plaza, A.; Merlet, G.; Hasanoglu, A.; Isaacs, M.; Sanchez, J.; Romero, J. Separation of Butanol from ABE Mixtures by Sweep Gas Pervaporation Using a Supported Gelled Ionic Liquid Membrane: Analysis of Transport Phenomena and Selectivity. *J. Membr. Sci.* **2013**, *444*, 201−212.

(6) Luo, R. W.; Ding, H.; Lyu, J. F.; Fu, T. Y.; Bai, P.; Guo, X. H.; Tsapatsis, M. Fabrication of a Sandwiched Silicalite-1 Membrane in a 2D Confined Space for Enhanced Alcohol/Water Separation. *Chem. Commun.* **2020**, *56*, 12586−12588.

(7) Contreras-Martinez, J.; Mohsenpour, S.; Ameen, A. W.; Budd, P. M.; Garcia-Payo, C.; Khayet, M.; Gorgojo, P. High-Flux Thin Film Composite PIM-1 Membranes for Butanol Recovery: Experimental Study and Process Simulations. *ACS Appl. Mater. Interfaces* **2021**, *13*, 42635−42649.

(8) Si, Z.; Li, J.; Ma, L.; Cai, D.; Li, S.; Baeyens, J.; Degreve, J.; Nie, J.; Tan, T.; Qin, P. The Ultrafast and Continuous Fabrication of a Polydimethylsiloxane Membrane by Ultraviolet-induced Polymerization. *Angew. Chem., Int. Ed.* **2019**, *58*, 17175−17179.

(9) Fan, H. W.; Shi, Q.; Yan, H.; Ji, S. L.; Dong, J. X.; Zhang, G. J. Simultaneous Spray Self-Assembly of Highly Loaded ZIF-8-PDMS Nanohybrid Membranes Exhibiting Exceptionally High Biobutanol-Permselective Pervaporation. *Angew. Chem., Int. Ed.* **2014**, *53*, 5578−5582.

(10) Zhang, G.; Cheng, H. F.; Su, P. C.; Zhang, X.; Zheng, J. H.; Lu, Y. H.; Liu, Q. L. PIM-1/PDMS Hybrid Pervaporation Membrane for High-Efficiency Separation of n-Butanol-Water Mixture under Low Concentration. *Sep. Purif. Technol.* **2019**, *216*, 83−91.

(11) Zhu, T. Y.; Yu, X.; Yi, M.; Wang, Y. Facile Covalent Crosslinking of Zeolitic Imidazolate Framework/Polydimethylsiloxane Mixed Matrix Membrane for Enhanced Ethanol/Water Separation Performance. *ACS Sustain. Chem. Eng.* **2020**, *8*, 12664−12676.

(12) Yang, D. C.; Tian, D. X.; Xue, C.; Gao, F.; Liu, Y.; Li, H.; Bao, Y. M.; Liang, J. J.; Zhao, Z. B.; Qiu, J. S. Tuned Fabrication of the Aligned and Opened CNT Membrane with Exceptionally High Permeability and Selectivity for Bioalcohol Recovery. *Nano Lett.* **2018**, *18*, 6150−6156.

(13) Fan, H. W.; Xie, Y. F.; Li, J. C.; Zhang, L.; Zheng, Q. Y.; Zhang, G. J. Ultra-high Selectivity COF-based Membranes for Biobutanol Production. *J. Mater. Chem. A* **2018**, *6*, 17602−17611.

(14) Zhao, J.; Zhu, Y. W.; He, G. G.; Xing, R. S.; Pan, F. S.; Jiang, Z. Y.; Zhang, P.; Cao, X. Z.; Wang, B. Y. Incorporating Zwitterionic Graphene Oxides into Sodium Alginate Membrane for Efficient Water/Alcohol Separation. *ACS Appl. Mater. Interfaces* **2016**, *8*, 2097−2103.

(15) Xu, L. H.; Li, S. H.; Mao, H.; Zhang, A. S.; Cai, W. W.; Wang, T.; Zhao, Z. P. An Advanced Necklace-like Metal Organic Framework with an Ultrahighly Continuous Structure in the Membrane for Superior Butanol/Water Separation. *J. Mater. Chem. A* **2021**, *9*, 11853−11862.

(16) Li, W.; Zhang, Y.; Li, Q.; Zhang, G. Metal−organic Framework Composite Membranes: Synthesis and Separation Applications. *Chem. Eng. Sci.* **2015**, *135*, 232−257.

(17) Li, W.; Su, P.; Li, Z.; Xu, Z.; Wang, F.; Ou, H.; Zhang, J.; Zhang, G.; Zeng, E. Ultrathin Metal-Organic Framework Membrane Production by Gel-vapour Deposition. *Nat. Commun.* **2017**, *8*, 406.

(18) Li, Y.; Zhang, X.; Chen, X.; Tang, K. J.; Meng, Q.; Shen, C.; Zhang, G. L. Zeolite Imidazolate Framework Membranes on Polymeric Substrates Modified with Poly(vinyl alcohol) and Alginate Composite Hydrogels. *ACS Appl. Mater. Interfaces* **2019**, *11*, 12605−12612.

(19) Zhang, X.; Zeng, Y.; Shen, C.; Fan, Z.; Meng, Q.; Zhang, W.; Zhang, G.; Gao, C. In Situ Assembly of Polyamide/Fe(BTC) Nanocomposite Reverse Osmosis Membrane Assisted by Fe^{3+}-Polyphenolic Complex for Desalination. *ACS Appl. Mater. Interfaces* **2021**, *13*, 48679−48690.

(20) Yuan, S.; Feng, L.; Wang, K. C.; Pang, J. D.; Bosch, M.; Lollar, C.; Sun, Y. J.; Qin, J. S.; Yang, X. Y.; Zhang, P.; Wang, Q.; Zou, L. F.; Zhang, Y. M.; Zhang, L. L.; Fang, Y.; Li, J. L.; Zhou, H. C. Stable Metal-Organic Frameworks: Design, Synthesis, and Applications. *Adv. Mater.* **2018**, *30*, 1704303.

(21) Feng, D.; Wang, K.; Wei, Z.; Chen, Y. P.; Simon, C. M.; Arvapally, R. K.; Martin, R. L.; Bosch, M.; Liu, T. F.; Fordham, S. Kinetically Tuned Dimensional Augmentation as a Versatile Synthetic Route Towards Robust Metal−Organic Frameworks. *Nat. Commun.* **2014**, *5*, 5723.

(22) Hwang, J.; Ejsmont, A.; Freund, R.; Goscianska, J.; Schmidt, B.; Wuttke, S. Controlling the Morphology of Metal-organic Frameworks and Porous Carbon Materials: Metal Oxides as Primary Architecture-directing Agents. *Chem. Soc. Rev.* **2020**, *49*, 3348−3422.

(23) Qin, L.; Gao, M. Z.; Zhang, M. Y.; Li, X.; Ru, R.; Luo, H. L.; Zhang, G. L. Bioinspired Assembly of Double Honeycomb-Like Hierarchical Capsule Confined Encapsulation with Functional Micro/Nanocrystals. *Small* **2020**, *16*, 2004692.

(24) Dang, S.; Zhu, Q. L.; Xu, Q. Nanomaterials Derived from Metal−Organic Frameworks. *Nat. Rev. Mater.* **2018**, *3*, 17075.

(25) Wang, C. H.; Kim, J.; Tang, J.; Kim, M.; Lim, H.; Malgras, V.; You, J.; Xu, Q.; Li, J. S.; Yamauchi, Y. New Strategies for Novel MOF-derived Carbon Materials Based on Nanoarchitectures. *Chem.* **2020**, *6*, 19−40.

(26) Qin, L.; Xu, Z. H.; Zheng, Y. L.; Li, C.; Mao, J. W.; Zhang, G. L. Confined Transformation of Organometal-Encapsulated MOFs into Spinel $CoFe_2O_4$/C Nanocubes for Low-Temperature Catalytic Oxidation. *Adv. Funct. Mater.* **2020**, *30*, 1910257.

(27) Qin, L.; Ru, R.; Mao, J. W.; Meng, Q.; Fan, Z.; Li, X.; Zhang, G. L. Assembly of MOFs/polymer hydrogel derived Fe_3O_4-CuO@ hollow Carbon Spheres For Photochemical Oxidation: Freezing Replacement for Structural Adjustment. *Appl. Catal., B* **2020**, *269*, 118754.

(28) Chaikittisilp, W.; Ariga, K.; Yamauchi, Y. A New Family of Carbon Materials: Synthesis of MOF-derived Nanoporous Carbons and their Promising Applications. *J. Mater. Chem. A* **2013**, *1*, 14−19.
(29) Masoomi, M. Y.; Morsali, A. Applications of Metal−Organic Coordination Polymers as Precursors for Preparation of Nanomaterials. *Coordin. Chem. Rev.* **2012**, *256*, 2921−2943.
(30) Wang, H. F.; Chen, L. Y.; Pang, H.; Kaskel, S.; Xu, Q. MOF-derived Electrocatalysts for Oxygen Reduction, Oxygen Evolution and Hydrogen Evolution Reactions. *Chem. Soc. Rev.* **2020**, *49*, 1414−1448.
(31) Si, Z. H.; Cai, D.; Li, S. F.; Zhang, C. W.; Qin, P. Y.; Tan, T. W. Carbonized ZIF-8 Incorporated Mixed Matrix Membrane for Stable ABE Recovery from Fermentation Broth. *J. Membr. Sci.* **2019**, *579*, 309−317.
(32) Saraswathi, M.; Nagendran, A.; Rana, D. Tailored Polymer Nanocomposite Membranes Based on Carbon, Metal Oxide and Silicon Nanomaterials: A Review. *J. Mater. Chem. A* **2019**, *7*, 8723−8745.
(33) Thomas, M. L.; Yamanaka, K.; Ohta, T.; Byon, H. R. A Perfluorinated Moiety-grafted Carbon Nanotube Electrode for the Non-aqueous Lithium−oxygen Battery. *Chem. Commun.* **2015**, *51*, 3977−3980.
(34) Kapri, S.; Maiti, S.; Bhattacharyya, S. Lemon Grass Derived Porous Carbon Nanospheres Functionalized for Controlled and Targeted Drug Delivery. *Carbon* **2016**, *100*, 223−235.
(35) Li, Y. B.; Wee, L. H.; Martens, J. A.; Vankelecom, I. F. J. ZIF-71 as a Potential Filler to Prepare Pervaporation Membranes for Bio-alcohol Recovery. *J. Mater. Chem. A* **2014**, *2*, 10034−10040.
(36) He, M.; Yao, J.; Liu, Q.; Wang, K.; Chen, F.; Wang, H. Facile Synthesis of Zeolitic Imidazolate Framework-8 from a Concentrated Aqueous Solution. *Microporous Mesoporous Mater.* **2014**, *184*, 55−60.
(37) Park, K. S.; Ni, Z.; Cote, A. P.; Choi, J. Y.; Huang, R.; Uribe-Romo, F. J.; Chae, H. K.; O'Keeffe, M.; Yaghi, O. M. Exceptional Chemical and Thermal Stability of Zeolitic Imidazolate Frameworks. *Proc. Natl. Acad. Sci. U.S.A.* **2006**, *103*, 10186−10191.
(38) Jing, X.; Guo, Z. Durable Lubricant-Impregnated Surfaces for Water Collection under Extremely Severe Working Conditions. *ACS Appl. Mater. Interfaces* **2019**, *11*, 35949−35958.
(39) Zhou, X.; Zou, Y.; Ma, J.; Cheng, X.; Li, Y.; Deng, Y.; Zhao, D. Cementing Mesoporous ZnO with Silica for Controllable and Switchable Gas Sensing Selectivity. *Chem. Mater.* **2019**, *31*, 8112−8120.
(40) Wu, X. C.; Wei, W.; Jiang, W. J.; Caro, J.; Huang, A. Dynamics of Xylene Isomers in MIL-53 (Al) MOF Probed by Solid State 2H NMR. *Angew. Chem., Int. Ed.* **2018**, *130*, 15354−15358.
(41) Mao, H.; Zhen, H.-G.; Ahmad, A.; Li, S.-H.; Liang, Y.; Ding, J.-F.; Wu, Y.; Li, L.-Z.; Zhao, Z.-P. Highly Selective and Robust PDMS Mixed Matrix Membranes by Embedding Two-dimensional ZIF-L for Alcohol Permselective Pervaporation. *J. Membr. Sci.* **2019**, *582*, 307−321.
(42) Cai, D.; Hu, S.; Miao, Q.; Chen, C. J.; Chen, H. D.; Zhan, C. W.; Li, P.; Qin, P. Y.; Tan, T. W. Two-stage Pervaporation Process for Effective in Situ Removal Acetone-Butanol-Ethanol from Fermentation Broth. *Bioresour. Technol.* **2017**, *224*, 380−388.
(43) Wang, N. X.; Shi, G. X.; Gao, J.; Li, J.; Wang, L.; Guo, H. X.; Zhang, G. J.; Ji, S. L. MCM-41@ZIF-8/PDMS Hybrid Membranes with Micro- and nanoscaled Hierarchical Structure for Alcohol Permselective Pervaporation. *Sep. Purif. Technol.* **2015**, *153*, 146−155.

https://doi.org/10.1021/acsomega.2c00881
ACS Omega 2022, 7, 15786−15794